positions and some oxygen positions are maintained in a rotation of 90° about the *c* axis, the twinning results only in a difference in the remaining oxygen distribution, producing a random instead of an ordered arrangement. While a truly tetragonal phase may exist, our results suggest that it is very easy to identify a twinned orthorhombic crystal as this tetragonal phase.

It is grafitying that our minute crystal is representative of the bulk polycrystalline specimen. We have found the powder pattern simulation to be a valuable adjunct to the single-crystal study.

Although our results support the structure proposed by the neutron diffraction study, there are some important differences in the occupancies of the oxygen sites. In this study three of the four oxygen positions are fully occupied, with the fourth, O(1), only 72% occupied. In the neutron diffraction study two oxygen sites were partially occupied: O(1) at 92% and O(4) at 95%. This may point out the importance that sample history has on the distribution of oxygen in such materials, without significantly affecting the stoichiometry. The composition of our material is $Ba_2YCu_3O_{6.7}$ compared to $Ba_2YCu_3O_{6.81}$ from the neutron data. The unusual thermal parameters obtained for the partially occupied oxygen positions in both this X-ray study and the neutron structure should be noted. This is the only site in the structure where there seems to be substantial anisotropy in the thermal motions, with the biggest deviations along the *a* axis, toward the unoccupied oxygen site.

The existence of both Cu^{3+} and Cu^{2+} in this material can be deduced from the stoichiometry of the material and a consideration of the charge balance. Since it has been proposed that this influences the high-temperature superconductivity of the material,[8] we have examined the observed electron density about the copper sites in order to try to verify the existence of the two oxidation states of the Cu. There is a 10% lower integrated density about Cu(1) than Cu(2). Cu(2) has a more regular square-planar arrangement of oxygens, with a fifth long bond of 2.350 (14) Å, and thus appears to be similar to a common Cu^{2+} configuration. The arrangement of the four oxygen atoms about Cu(1) is distorted, involving short Cu(1)–O(2) distances of 1.815 (14) Å. This, combined with the lower electron density, is suggestive that the Cu(1) site might contain at least a partial occupancy by Cu^{3+}.

Supplementary Material Available: Table SI of anisotropic thermal parameters for the orthorhombic structure (1 page); tables of observed and calculated structure factors for both structures (2 pages). Ordering information is given on any current masthead page.

(8) Pauling, L. *Phys. Rev. Lett.* **1987**, *59*, 225.

Contribution from Corporate Research,
Exxon Research and Engineering Company, Annandale, New Jersey 08801

Studies on the Low-Temperature Synthesis and Surface Chemistry of Iron Monoxide

David J. C. Yates* and James A. McHenry

Received November 17, 1986

Thin films of FeO have been made by the action of steam on iron foils or flat coupons at temperatures between 540 and 800 °C. Growth rates at 800 °C are quite high, about 20 μm/h. We have found that the time of treatment for any given thickness is critical, at constant temperature and flow rates of steam. For example, a foil of thickness 127 μm was essentially all converted to FeO by a 3-h treatment at 800 °C. At longer time, the outside of the foil begins to convert to Fe_3O_4, and at still longer times, the sample becomes entirely Fe_3O_4. The effect of added oxygen has been studied, and it has been found that the amount of oxygen normally dissolved in water presents no problem. However, higher amounts of oxygen, while increasing the growth rates of the FeO, also produce some Fe_2O_3. Iron monoxide is an active catalyst for the formation of filamentous carbon (from hydrocarbons at 700 °C), being at least 1 order of magnitude more active than iron and nickel foils at these temperatures. The basis for this high activity has been investigated and is probably due to the fact that FeO very rapidly reduces to porous iron while the coking is occurring, which must then be of correct porosity to form carbon filaments in profusion.

Introduction

Although there has been extensive publication on the formation and synthesis of the oxides of iron,[1-14] little work has been done on the synthesis of ferrous oxide (iron monoxide, FeO, Wüstite) from metallic iron at temperatures below 1000 °C.

We have found that it is possible to synthesize FeO starting from either pure iron foils or from mild steel by the action of steam alone at temperatures above 540 °C. At the lower temperatures (580–650 °C) the reaction rate was very low, resulting in very small weight gains, so identification of the product of the reactions was done by Auger analysis.[15] At higher temperatures, for example 800 °C, we found it possible to convert all of a 0.005-in. iron foil into FeO by a short steam treatment. In addition, we have shown by X-ray measurements that after all the metallic iron had been converted to FeO, continuing steam treatment began transforming the outside of the FeO to Fe_3O_4. Longer treatments converted all of the FeO to pure Fe_3O_4, as shown by weight changes and confirmed by X-ray analysis.

Out interest in FeO was aroused by its very high efficiency as a catalyst for the production of filamentous carbon,[16] and a patent

(1) Mellor, J. W. (revised by Parkes, G. D.) *Mellor's Modern Inorganic Chemistry*; Longmans, Green: London, 1967.
(2) Darken, L. S.; Gurry, R. W. *J. Am. Chem. Soc.* **1945**, *67*, 1398.
(3) Sidgwick, N. V. *The Chemical Elements and Their Compounds*; Oxford University Press: Oxford, England, 1950.
(4) Hansen, M.; Anderko, K. *Constitution of Binary Alloys*, 2nd ed.; McGraw-Hill: New York, 1958.
(5) Hazen, R. M.; Jeanloz, R. *Rev. Geophys. Space Phys.* **1984**, *22*, 37.
(6) Carter, R. E. *J. Am. Ceram. Soc.* **1959**, *42*, 324.
(7) Will, G.; Hinze, E.; Nuding, W. *Phys. Chem. Miner.* **1980**, *6*, 157.
(8) Koch, F. B.; Fine, M. E. *J. Appl. Phys.* **1967**, *38*, 1470.
(9) Koch, F. B.; Cohen, J. B. *Acta Crystallogr., Sect. B: Struct. Crystallogr. Cryst. Chem.* **1969**, *B25*, 285.
(10) Andersson, B.; Sletnes, J. O. *Acta Crystallogr., Sect. A: Cryst. Phys., Diffr., Theor. Gen. Crystallogr.* **1977**, *A33*, 268.
(11) Hayakawa, M.; Cohen, J. B.; Reed, T. B. *J. Am. Ceram. Soc.* **1972**, *55*, 160.
(12) Kugel, G.; Carabatos, C.; Hennion, B.; Prevot, B.; Revcolevschi, A.; Tocchetti, D. *Phys. Rev. B: Solid State* **1977**, *16*, 378.
(13) Berthon, J.; Revcolevschi, A.; Morikawa, H.; Touzelin, B. *J. Cryst. Growth* **1979**, *47*, 736.
(14) Chipman, J.; Marshall, S. *J. Am. Chem. Soc.* **1940**, *62*, 299.
(15) Seo, M.; Lumsden, J. B.; Staehle, R. W. *Surf. Sci.* **1975**, *50*, 541.
(16) Baker, R. T. K.; Alonzo, J. R.; Dumesic, J. A.; Yates, D. J. C. *J. Catal.* **1982**, *77*, 74.

0020-1669/87/1326-3193$01.50/0

has recently[17] been issued covering both its low-temperatue synthesis and its subsequent use in filamentous-carbon formation.

Experimental Section

Most of the experiments were done in a fused silica reactor (2.5 cm in diameter, 90 cm in length) that was externally heated via a three-zone furnace, of overall length 61 cm. The center zone was 46 cm long, and by careful adjustment procedures the whole 46 cm could be held at a set temperature to within ±1 °C.

To enable samples to be loaded into the furnace at reproducible positions in the tube and facilitate their removal without disturbing the samples, a special holder was constructed. This consists of a series of six sections of silica tubing, each 3 cm in length and 1.5 cm in diameter, held together with a fused silica rod, the latter being long enough to reach to the exit of the reactor.[16] This arrangement also had the advantage that the samples were held so that their maximum surface area was exposed to the gas phase.

The iron used for these experiments was obtained from two sources. One, in thicknesses of 0.002 and 0.005 in. (50.8 and 127 μm) was obtained from the Materials Research Corp. of Orangeburg, NY, and was 99.99% pure. The other, in thicknesses of 0.1 and 0.25 mm (100 and 250 μm) and of purity 99.9975% (Puratronic grade), was from Johnson Matthey Inc. (Aesar Group), Seabrook, NH.

In some experiments low-carbon steel sheet (Anal. Found: C, 0.15 (maximum); Mn 0.9–1.3; S, 0.25–0.35) was used, of thicknesses 0.013 and 0.050 in. (330 and 1270 μm). In addition, some of the later experiments were done in an Inconel (iron–nickel alloy) reactor, of geometry similar to that of the silica reactor, to eliminate possible effects on FeO synthesis derived from any possible removal of silica from the reactor walls.

The water was always distilled prior to use and either was pressured directly into the quartz wool packing at the inlet of the reactor[16] or was pumped in at a known rate from an accurate piston pump (Isco, Inc. Lincoln, NE). In most cases, the water was rendered oxygen-free by purging extensively with either N_2 or Ar before use, although in some experiments nondeaerated water was used. To study in more detail the effect of oxygen, in some experiments air was added at known flow rates to the steam. During most experiments, small N_2 flows were added to the steam to maintain an even flow of water at the exit of the reactor.

Experiments studying weight gain of various iron and steel samples are presented in Table I. Compositional analyses were done of the surface and near-surface regions by Auger spectroscopy[15,18,19] and of the bulk by X-ray diffraction.

The Auger elemental analyses were obtained by using the known relative sensitivities[15,18] of the peaks of iron and oxygen. Small samples of the reactor foil were inserted into the vacuum chamber of the spectrometer. After the initial spectrum was recorded, argon ion bombardment was begun and a series of spectra taken at various depths below the surface. As the Auger electrons we studied have energies below 1000 eV, their escape depth is typically[19] less than 50 Å. Hence, the information in the Auger spectrum is obtained from the surface and near-surface regions.

Other samples, both intact ones and also ones subsequently ground to powder, were examined by conventional X-ray techniques, and the results are summarized in Table II (supplementary material). The reason for measuring the sample spectra in the unground state is to determine the average composition of the as-reacted sample in the depth accessible to X-rays. For our samples, M. A. Modrick calculated that 80% of the X-ray information is obtained from the top 2 μm of the sample surface. This was of great value in our understanding of the nature of the phases seen after the thin foils were fully converted to FeO, as will become apparent in the Discussion.

Some samples were examined in our scanning electron microscope, both in the secondary mode and in the backscattering mode. Point elemental analyses of the samples were also done in situ in the microscope via the X-rays emitted from the elements contained in the sample. Elements with atomic numbers of 6 and higher could be detected by our analyzer.

Results

A complete summary of the experimental conditions, water flow rates, dilution gas, etc. is given in Table I.

From the weight gains of the individual samples in the final experiments, the values of x in FeO_x were calculated and are given in Tables I and II (Table II is supplementary material). As the samples were exposed to the steam on both sides, the weight gains (as long as x was less than unity) could be readily converted into thickness of the FeO, and values are given for each sample as total thickness in micrometers and also the rate in micrometers per hour, assuming that the rate was linear with time. Given in the last column are the average values in micrometers per hour for samples of a given thickness, in cases where more than one sample of a given thickness was used in one experiment.

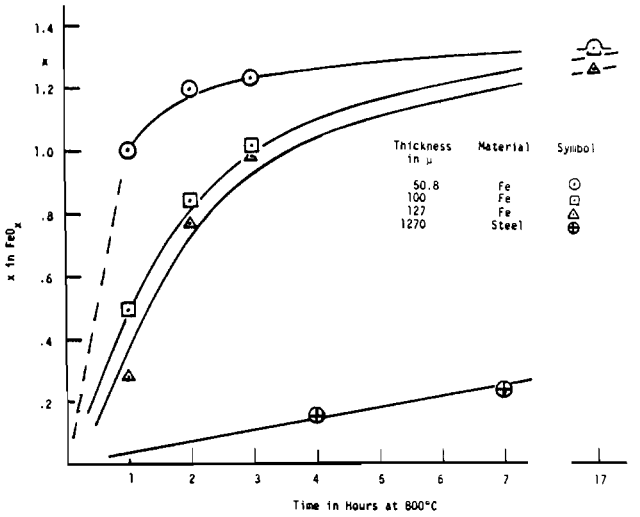

Figure 1. Rate of formation of FeO at 800 °C as a function of time.

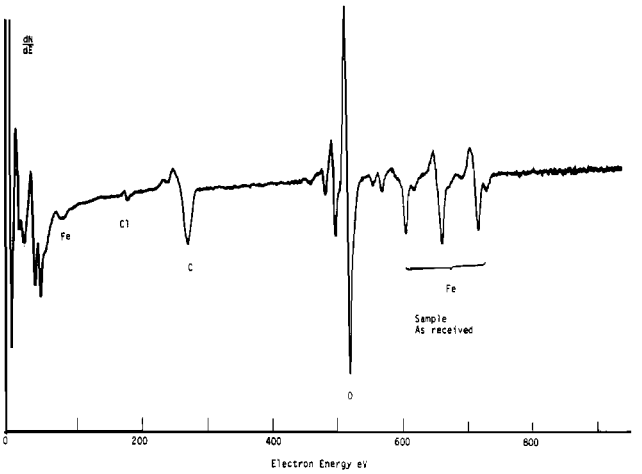

Figure 3. Auger spectrum of sample of FeO_x made with water vapor at 800 °C for 3 h.

All the experiments in the first part of Table I were done at 800 °C, for varying times, and (except run 129) were done with deaerated water and with varying nitrogen flows. Two other variables, studied in the last five experiments in Table I, were the effect of adding small amounts of air to the steam/N_2 mixtures and the effect of temperature on the reaction in steam/N_2 mixtures.

The X-ray diffraction data are summarized in Table II, and it was found that, unless air was added on purpose (runs 124 and 125), the only phases found were FeO and Fe_3O_4. In the presence of air, Fe_2O_3 could be visually detected by a color change as well as by X-ray examination.

The conversion to FeO is given in Figure 1 as a function of time of treatment at 800 °C. The effect of thickness is dramatically shown; in 1 h the 50.8-μm sample was fully converted to FeO, becoming pure Fe_3O_4 after a 17-h treatment. In 1 h, the 127-μm sample was only about one-third converted to FeO, while the conversion was extremely low with the 1270-μm sample. After 17 h, the 127-μm sample was close to being fully converted to Fe_3O_4, while the 1270-μm sample had an overall composition of $FeO_{0.23}$ after 7 h. The effect of varying the injection rate of liquid water at 800 °C is shown in Figure 2 (supplementary material).

(17) Yates, D. J. C.; Baker, R. T. K. U.S. Patent 4565683, Jan 1986.
(18) Davis, L. E. *Handbook of Auger Spectroscopy*, 2nd ed.; Physical Electronic Industries: Eden Prairie, MN, 1976.
(19) Chang, C. C. *Surf. Sci.* **1971**, *25*, 53.

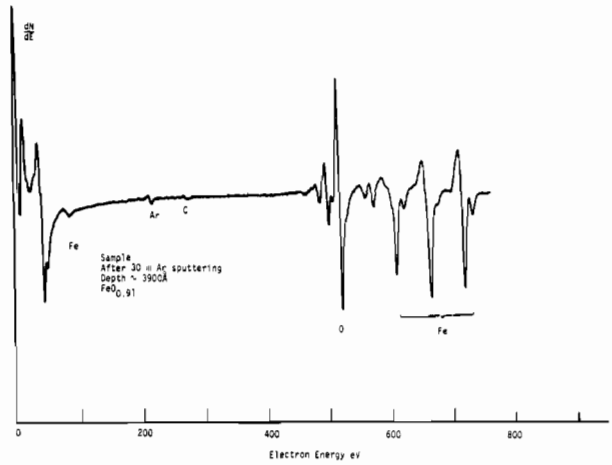

Figure 4. Auger spectrum of sample used in Figure 3, after sputtering for 30 min (~3900 Å).

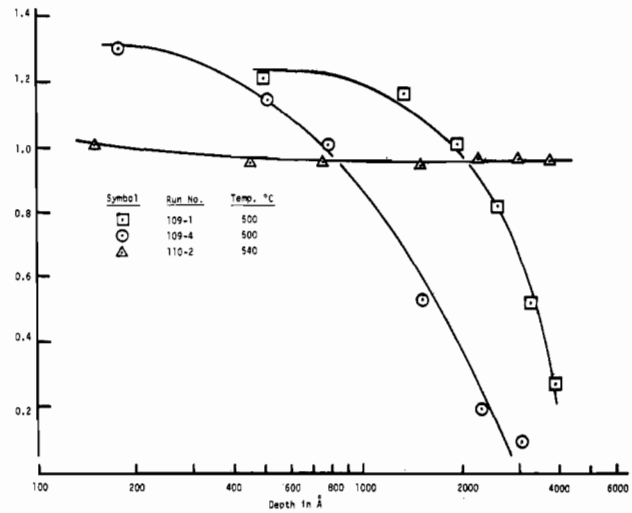

Figure 5. Composition–depth profile by Auger analysis.

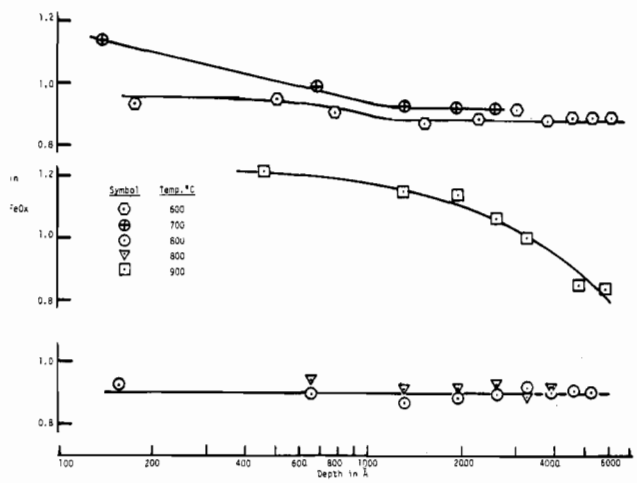

Figure 6. Composition–depth profile by Auger analysis.

Figure 3 shows a typical Auger spectrum of the samples as first inserted into the spectrometer. All showed small amounts of carbon, which is a normal handling contaminant. In all cases, the carbon was removed after a short Ar ion sputtering (e.g., 1–2 min) and so it is not a constituent of the FeO film. Figure 4 shows a spectrum typical of that found for an FeO sample at a depth of about 3900 Å, or 0.39 μm. It will be seen that, apart from very weak peaks of Ar and C, no elements other than Fe and O were present. The Auger spectra have been converted into atomic composition and are shown as FeO_x in Figures 5 and 6. It was expected from previous work[2-4] that FeO would not be formed at temperatures below about 560–570 °C. At 500 °C, this expectation was confirmed, as both samples treated at 500 °C showed a continuous drop in oxygen content with time of bombardment. However, there was an apparent discrepency with the 540 °C sample, as at depths down to about 3700 Å, the sample was of constant composition, close to that of FeO. This sample will be discussed later.

Figures 7–12 (Figures 9 and 10 are supplementary material) show the X-ray spectra recorded compared to standard spectra[20]

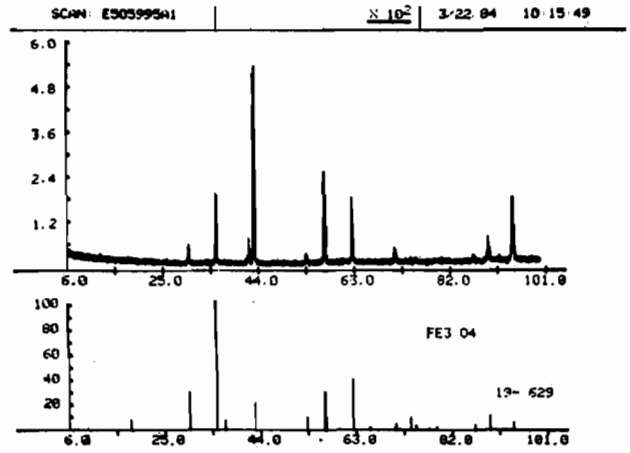

Figure 7. X-ray spectrum of sample 125-5 (unground) (upper) and reference spectrum of Fe_3O_4 (lower).

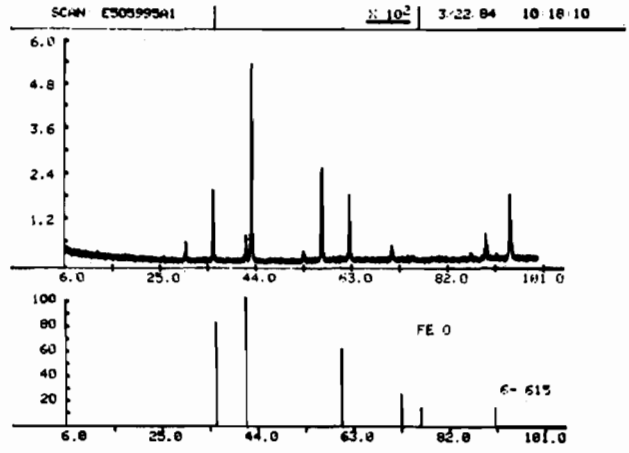

Figure 8. X-ray spectrum of sample 125-5 (unground) (upper) and reference spectrum of FeO (lower).

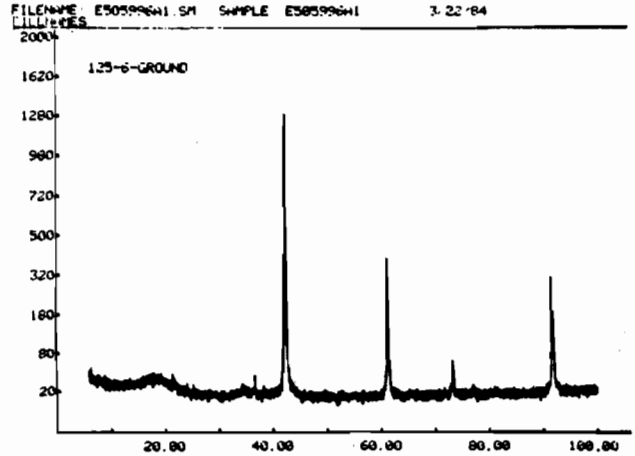

Figure 11. X-ray spectrum of sample 125-6 (ground).

(20) *Powder Diffraction File*; Inorganic Press, Joint Committee for Powder Diffraction Standards, International Center for Diffraction Data: Swarthmore, PA 19081, 1981.

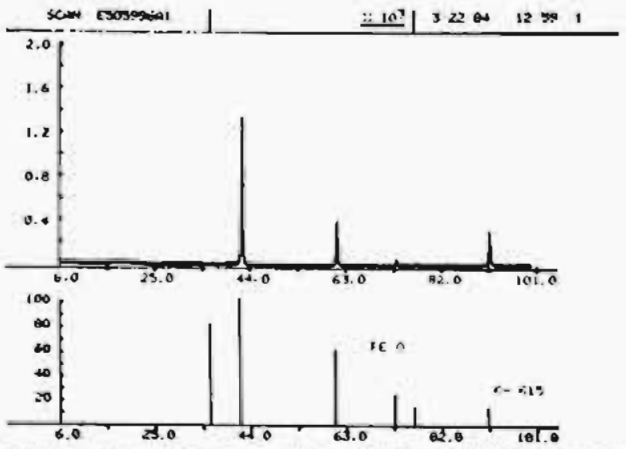

Figure 12. X-ray spectrum of sample 125-6 (ground) (upper) and reference spectrum of FeO (lower).

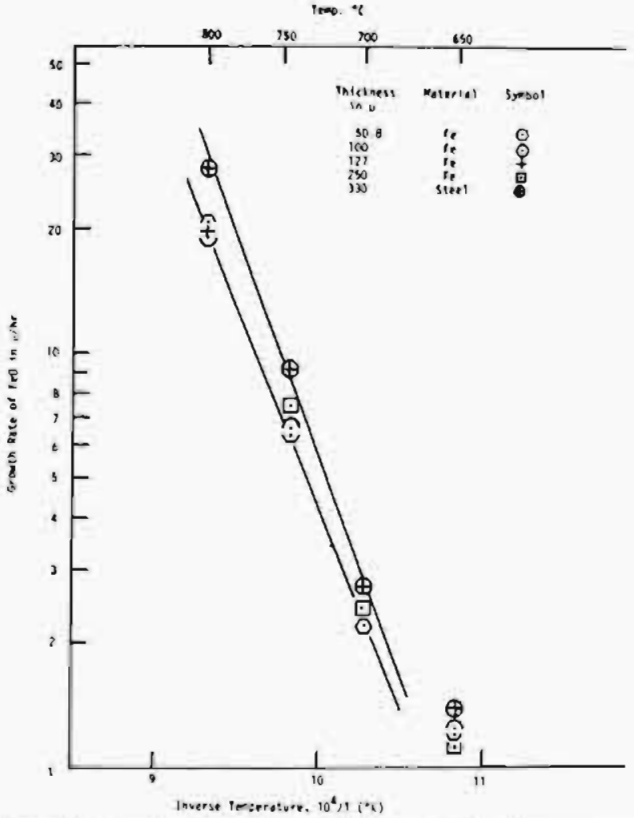

Figure 13. Variation of growth rate of FeO as a function of temperature.

for Fe, FeO, Fe_2O_3, and Fe_3O_4.

Figure 13 shows the data on the kinetics of growth of FeO as a function of temperature, thickness, and origin of the samples.

Figures 14–17 (Figures 16 and 17 are supplementary material) show the images obtained in the scanning electron microscope of the as-formed FeO and the topographical details of its reaction with ethane to form filamentous carbon.

Discussion

Gravimetric Data. A systematic study of the effects of time, temperature, flow rate of steam, added oxygen, etc. was performed by using multithickness samples in every experiment.

Rather than give the individual weight changes, we have converted them in Table I to the molar fraction of oxygen in FeO_x, assuming that only oxygen was added to the iron. This was based on preliminary X-ray and Auger data given earlier.[16]

The first series of experiments at 800 °C was done for varying times but at constant water (0.5 cm^3/min liquid) and nitrogen flows (50 cm^3/min). These are runs 115 and 122 (both done for 1 h to determine reproducibility), 119 (2 h), 114 (3 h), 128 (4 h), 129 (7 h), and 120 (17 h). The long run had to be done with a water flow of 0.33 cm^3/min, rather than 0.5 cm^3/min, as our pump capacity was not sufficient for this length of run at the higher flow. The data in these runs are plotted in Figure 1, and it will be seen that iron foils from both sources gave essentially the same conversion (100-μm foil was from Aesar, 127-μm foil was from Materials Research) when allowance was made for their thickness. For runs 115, 119, and 122, which gave the most precise

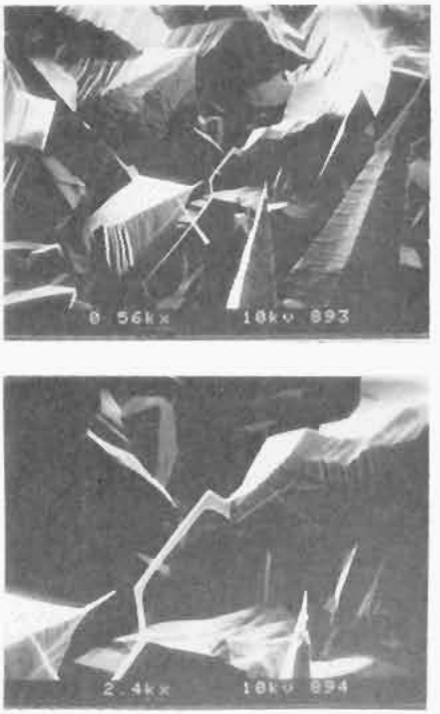

Figure 14. SEM photographs of crystalline surface structure of FeO (sample made at 800 °C): (upper) secondary image, 560× 1 cm representing 20 μm; (lower) secondary image, 2400×, 1 cm representing 5 μm.

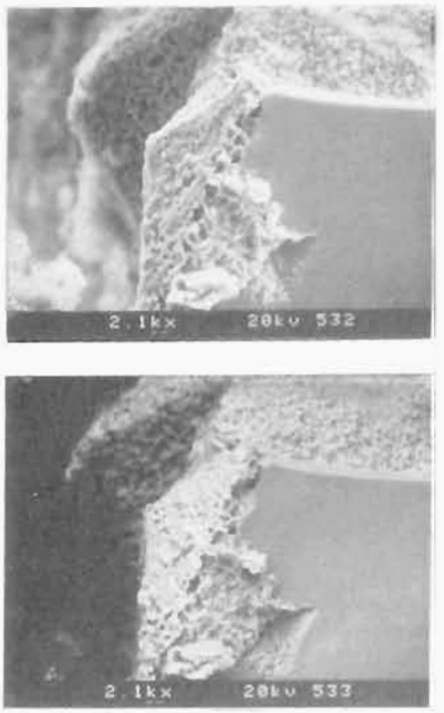

Figure 15. SEM photographs of fractured section of FeO after 10 min of coking (2100×, 1 cm representing 4.8 μm): (upper) secondary image; (lower) backscattered image. Note the porous structure that is created as the FeO is reduced to iron. The smooth area in the lower right hand corners is the fracture surface of FeO.

data, the growth rate for all thicknesses and both sources of iron foils was between 18 and 24.5 μm/h. Average values for four comparable runs (115, 122, 119, and 121) show reasonable agreement (22.38, 22.83, 22.75, and 21.65 μm/h), giving an average of 22.4 μm/h. It is of interest that the thin steel (330 μm) used in runs 122, 119, and 121 showed higher growth rates, the average being 27.1 μm/h. However, it is not certain at this time that this higher value is to be found for all geometries and thicknesses of steel. This is because the very thick (1270 μm), large (1 in. × 4 in.) coupons used in runs 128 and 129 gave a growth rate of 24.5 and 21.0 μm/h, or an average of 22.8 μm/h, essentially the same as for the pure iron foils.

The effect of the injection rate of the water was studied in a series of 1-h runs at 800 °C. The data are presented in Figure 2 (supplementary material) and show lower growth rates at both the highest and the lowest flow, with a broad maximum in rate between 0.5 and 1.5 cm^3/min. It is possible that the dropoff at higher rate is due to the steam not being fully up to temperature and that the dropoff at low injection rates is due to a relatively low rate of supply of the active-growth species, possibly due to insufficient mixing near the metal surface. Obviously, to make FeO from Fe, the water must dissociate, either into hydroxyl groups and hydrogen or possibly into oxygen and hydrogen. As the dissociation of water will be different both in the gas phase and for the initial Fe and growing FeO surface, it is obvious that the kinetics and growth mechanism of FeO are of great complexity and cannot be discussed with the data we have in hand.

Nevertheless, we have studied the growth rate of FeO as a function of temperature, even though we were unable to do the experiments under strictly comparable conditions. The first attempt we made was a comparison between 800 and 750 °C, both for a duration of 3 h with a water flow of 0.5 cm^3/min. However, the conversions at 800 °C in run 114 (see Table I) were above unity except for the 100-μm sample. As the latter should be *more* converted than the 127-μm sample, there is obviously some problem with the data on the 100-μm sample in this run. The final comparisons were done with run 123 (800 °C, 1 h), run 126 (750 °C, 3 h), run 127 (700 °C, 17 h), and run 130 (650 °C, 17 h). Figure 13 shows that the values for 800, 750, and 700 °C fall closely on two straight lines, one for all thicknesses and suppliers of iron foils and another for the 330-μm sheet steel. Clearly, the 650 °C data do not fit on this plot, and the reason for this is unknown. However, as discussed earlier, there are so many variables involved in the growth of FeO from steam that it is really quite surprising that there is a linear growth region at all.

Auger Data. Illustrative Auger spectra are shown in Figures 3 and 4. All samples showed small carbon peaks on insertion into the vacuum chamber. This was only a slight surface contamination, as the carbon disappeared after 1-min bombardment (rate about 130 Å/min). Measurement of the intensity of the oxygen peak at 503 eV and the iron peak at 703 eV enabled[15,18,19] the surface composition to be calculated at that particular depth.

The data are then expressed in terms of FeO_x, vs. depth of bombardment, and are given in Figures 5 and 6. Figure 5 shows that the two samples treated at 500 °C for 3 h (run 109, Table I) showed a continuous decrease in oxygen content down to the lowest level measured ($\rightarrow FeO_{0.2}$). Evidently, there is no indication of *any* stoichiometric oxide of iron formed under these conditions. The run at 540 °C for 3 h (run 110, Table I) in striking contrast showed a constant composition of $FeO_{0.96}$ at depths greater than 450 Å. This is in apparent contradiction with earlier work,[2-4] where the eutectic temperatures are given as 575[3] or 560 °C.[4] It is possible that our temperatures may be incorrect or simply that FeO can indeed be formed at 540 °C and that the techniques used by previous workers were not sensitive enough to detect the *very* small conversions to FeO which take place at these low temperatures. However, it should be noted that the previous studies were at equilibrium (at least that was the objective). In our experiments, it is clear that the FeO formed is not in an equilibrium situation, as continued exposure to steam gives Fe_3O_4 as the end product.

Figure 6 shows data obtained in runs from 600 to 900 °C. Except for the last, all runs show a long plateau of constant composition at values from $FeO_{0.8}$ to $Fe_{0.92}$ and in two cases essentially constant from 170 Å downwards. The reason for the nonuniform composition with the 900 °C sample is unknown, but this sample was made by use of water vapor, via nitrogen bubbled through a water reservoir, rather than by injection of liquid water.

X-ray Data. Although preliminary data had shown[16] that the surfaces of earlier samples were substantially pure FeO, detailed studies have been carried out only on samples of varying thickness in a given experiment.

All of the data obtained are given in Table II and in Figures 7–12. The standard[20] X-ray diffraction cards, giving both position and intensity of the peaks, of both iron and all of its oxides were used for interpretation. To differentiate the surface of the foils from the bulk, several samples were run both directly after the run, in the intact state, and also after grinding into powder. The latter gave the bulk composition and also helped to reduce the severe preferred orientation that was commonly observed in the unground foils. For both types of samples, with the X-ray source used, the depth of the sample accessible to X-rays was such that 80% of the signal originated from the top 2 μm of the sample surface.

At conversions less than unity, all the samples, mostly studied unground, showed only FeO in the X-ray spectrum. The lowest conversion for iron and steel samples was 0.153 (run 128-1) and the highest 0.86 (run 121-4). All of these spectra showed severe preferred orientation, as shown by the experimental relative intensities being very different from the standard spectra. Even when the sample was studied in the ground state (sample 125-6), the spectra, although showing pure FeO, showed very marked intensity changes (Figures 11 and 12). This is so extreme that the second most intense peak in the reference "stick" spectrum (lower half of Figure 12) was barefuly detectable in the experimental spectrum (Figure 11 and the upper half of Figure 12). The cause of this effect is not known but is probably due to a nonuniform packing of the ground FeO when it was pressed into the sample holder.

At higher conversions, but still less than unity, the samples showed both FeO and Fe_3O_4, e.g. runs 122–1 ($FeO_{0.89}$) and 114-4 ($FeO_{0.99}$). At conversions between unity and less than 1.33 (Fe_3O_4), the samples showed both FeO and Fe_3O_4, with Fe_3O_4 predominating in the unground state. An example is run 119-5 ($FeO_{1.21}$), where the unground sample had major peaks of Fe_3O_4 and minor peaks of FeO, while the relative compositions were reversed in the ground sample. A more extreme example was shown in samples 120-3 ($FeO_{1.27}$) and 120-6 ($FeO_{1.16}$), where both showed only Fe_3O_4 in the unground state and both FeO and Fe_3O_4 were recorded in the ground sample. Nevertheless, the ground samples of 120-3 and 120-6 still showed Fe_3O_4 to be the major peak (see Table II).

The same thing occurred in samples where small amounts of oxygen were added (run 125, 0.13% O_2). The spectrum of sample 125-5 ($FeO_{1.15}$) unground (Figure 7) showed predominantly Fe_3O_4, with only peaks due to FeO (Figure 8). It should be noted that the recorded spectrum showed very severe preferred orientation effects compared with the reference spectrum (Figure 7, upper and lower spectra). After grinding, the FeO peaks predominated in the spectrum while Fe_3O_4 gave weaker peaks (Figures 9 and 10). Due to this preferred orientation, even for ground samples containing both FeO and Fe_3O_4, a satisfactory analysis of the relative amounts of FeO and Fe_3O_4 could not be determined by X-ray diffraction. This was despite the fact that we were able to use pure FeO (many runs) and pure Fe_3O_4 (runs 141 and 156) as calibration standards. It is worth noting that the FeO in the JCPDC standards[20] contained up to 11% Fe_2O_3. This illustrates that pure FeO is not a readily available entity.

The above observations lead to the unambiguous conclusion that the initial growth process on contact of iron with steam at 800 °C is that FeO begins forming on the outside of the foil. As long as some metallic iron remains in the sample, *only* FeO is formed. When the sample is either mostly or fully converted to FeO, then Fe_3O_4 begins to grow on the outside surface of the FeO.

Table I. Experimental Data on FeO_x Production

(A) Constant Iron-Sample Thickness[a]

expt no.	temp, °C	time, h	H_2O flow, cm^3/min	N_2 flow, cm^3/min	x in FeO_x[b]	expt no.	temp, °C	time, h	H_2O flow, cm^3/min	N_2 flow, cm^3/min	x in FeO_x[b]
109	500	3	0.5	50	0.012	111[c]	950	0.5	0	50	0.072
					0.0074						0.044
					0.0023						0.034
					0.0013						0.028
110	540	3	0.5	50	0.017	112[d]	1000	0.42	0	50	0.053
					0.008						0.038
					0.010						0.027
					0.005						0.021

(B) Constant Temperature[e]

expt no.	time, h	H_2O flow, cm^3/min	N_2 flow, cm^3/min	starting thickness, μm[f]	x in FeO_x	total thickness of FeO, μm	rate, μm/h	av rate, μm/h
117	1	3	50	50.8	0.728		18.49	18.7
				127	0.360		22.86	19.7
				127	0.262		16.63	
				100	0.425		21.25	21.2
				50.8	0.744		18.89	
116	1	1.5	50	50.8	0.949		24.10	22.7
				127	0.405		25.72	25.2
				127	0.389		24.70	
				100	0.533		26.65	26.6
				50.8	0.841		21.36	
129[g]	7	0.5	50	1270 (lcs)	0.231	146.7	20.95	21.0[h]
				1270 (lcs)	0.233	147.9	21.13	
				1270 (lcs)	0.172	109.22	15.60	
128	4	0.5	50	1270 (lcs)	0.153	97.16	24.29	24.5[h]
				1270 (lcs)	0.156	99.06	24.76	
				1270 (lcs)	0.118	74.93	18.73	
114	3	0.5	50	50.8	1.225			
				50.8	1.196			
				127	1.016	~64	~21	
				100	0.993	49.65	16.6	
138	2	0.5	50	100	1.066	>50	>25	
	0.17			100	1.118			
119	2	0.5	50	50.8	1.19			
				127	0.757	48.07	24.03	24.6
				127	0.796	50.55	25.27	
				100	0.838	41.9	20.95	20.9
				50.8	1.210			
				330 (lcs)	0.289	47.71	23.86	23.9
115	1	0.5	50	50.8	0.933		23.70	23.7
				127	0.268		17.02	18.0
				127	0.301		19.11	
				100	0.491		24.55	24.5
				50.8	1.07		>25	
122	1	0.5	50	50.8	0.892		22.73	23.6
				127	0.373		23.68	23.7
				100	0.430		21.50	21.2
				100	0.420		21.00	
				50.8	0.964		24.48	
				330 (lcs)	0.201		33.18	33.2
121	2	0.5	231	50.8	1.18			
				127	0.71	45.02	22.50	21.9
				127	0.67	42.61	21.3	
				100	0.858	42.90	21.4	21.4
				50.8	1.19			
				330 (lcs)	0.292	48.21	24.1	24.1
120	17	0.33	26	50.8	1.335			
				127	1.265			
				127	1.268			
				100	1.323			
				50.8	1.335			
				330 (lcs)	1.162			
123	1	0.33	26	50.8	0.758		19.25	19.0
				127	0.308		19.56	19.6
				100	0.457		22.85	20.7
				100	0.370		18.5	
				50.8	0.74		18.77	

Table I (Continued)

expt no.	time, h	H_2O flow, cm^3/min	N_2 flow, cm^3/min	starting thickness, μm[f]	x in FeO_x	total thickness of FeO, μm	rate, $\mu m/h$	av rate, $\mu m/h$
				330 (lcs)	0.169		27.90	27.9
156	21 h 32 m	0.27	50	50.8	1.338			
141	22	0.27	26	100	1.325			
				100	1.343			
118	1	0.2	0	50.8	0.713		18.1	17.6
				127	0.264		16.76	19.2
				127	0.34		21.65	
				100	0.378		18.90	18.9
				50.8	0.677		17.2	
124[i]	1	0.5	50 (air)	50.8	1.336			
				127	1.122			
				100	1.198			
				100	1.15			
				50.8	1.32			
				330 (lcs)	0.424		70.0	70
125[j]	1	0.5	231 (N_2), 5.9 (air)	50.8	1.301			
				100	0.943		47.15	
				100	0.871		43.55	
				100	0.658		32.9	
				50.8	1.147			
				330 (lcs)	0.181		29.88	

(C) Varying Temperature and Iron-Sample Source

expt. no.	time, h	H_2O flow, cm^3/min	N_2 flow, cm^3/min	starting thickness, μm[n]	x in FeO_x	total thickness of FeO, μm	rate, $\mu m/h$	av rate, $\mu m/h$
126[k]	3	0.5	50	50.8	0.78	19.79	6.59	6.6
				250	0.181	22.62	7.54	7.54
				100	0.367	18.35	6.12	6.35
				100	0.395	19.75	6.58	
				50.8	...	...	...	
				330 (lcs)	0.164	27.08	9.02	9.02
127[l]	17	0.33	26	50.8	1.203			
				250	0.33	41.37	2.43	2.43
				100	0.736	36.8	2.16	2.19
				100	0.757	37.8	2.23	
				50.8	1.23			
				330 (lcs)	0.282	46.56	2.74	2.74
130[m]	17	0.33	26	50.8	0.781	19.84	1.16	1.24
				250	0.154	19.25	1.13	1.13
				100	0.430	21.50	1.26	1.20
				100	0.390	19.50	1.14	
				50.8	0.891	22.63	1.32	
				330 (lcs)	0.143	23.61	1.38	1.38

[a] All the iron samples were of starting thickness 127 μm in this part; source Materials Research Corp. (see Experimental Section). [b] Calculated from weight gain after treatment. The first entry in the table for a given experiment is for the sample nearest the inlet of the reactor; the last is closest to the exit. [c] Water vapor was used here; the nitrogen at 50 cm^3/min was passed through water at room temperature. [d] Water vapor only, as used in experiment 111. [e] The temperature was 800 °C for all experiments in this part. [f] Two sources of pure iron were used in this part, 50.8- and 127-μm samples were from Materials Research Corp. and 100-μm samples from Johnson Matthey Inc. Two thicknesses of low-carbon steel (lcs) were used, 330 and 1270 μm. For details see Experimental Section. [g] Normal water used in the Isco pump, i.e. nondeaerated. [h] Calculated from samples 1 and 2. [i] Note: All samples were reddish, except the last one, sample 6, which was black. [j] Note: The front half of the first sample was reddish; the back half of this sample and all other samples was gray. [k] Temperature 750 °C. [l] Temperature 700 °C. [m] Temperature 650 °C. [n] Two sources of pure iron were used in this part, 50.8 μm from Materials Research Corp. and 100 and 250 μm from Johnson Matthey Inc. One thickness of low-carbon steel (lcs) was used, 330 μm. For details see Experimental section.

At long times, and with samples 100 μm and thinner, the end product is pure Fe_3O_4, all of the FeO having been oxidized. This implies that the iron must diffuse outward through the FeO until it is all consumed. This predicts that FeO made from steam should be on the excess iron side of the stoichiometry. This is certainly the case in all of the samples that we studied by Auger spectroscopy in Figures 5 and 6. After it consumes all of the metallic iron, the steam begins to convert the outside surface of the FeO, probably by diffusion of oxygen inward through the growing Fe_3O_4. To prove this, marker experiments would have to be done, which, however, are not planned at this time.

As part of our efforts to understand the effect of oxygen, experiments were done with gaseous oxygen added to the steam. The first way this was studied was by not degassing the water used to form the steam (run 129). The data on growth rate, appearance of samples, etc. were essentially the same as those of run 128, where normally deaerated water was used. Both runs were done with large (1 in. × 4 in.) mild steel specimens in the Inconel reactor. The effects of known amounts of added oxygen (via air additions) are given in runs 124 (1.44% O_2) and 125 (0.13% O_2). In run 124, the tops of all of the samples were reddish (i.e. Fe_2O_3) except sample 6, which was dark gray. The X-ray diffraction data showed that sample 3 on the upper brown side was pure Fe_2O_3, while the lower gray side of the same sample was mixture of mainly FeO and also some Fe_3O_4, but not Fe_2O_3. Sample 5, on the red unground side, showed mainly Fe_2O_3, but with some Fe_3O_4.

After grinding, the bulk composition was found to be Fe_3O_4, with a trace of Fe_2O_3. Sample 6, in contrast, which had no reddisch coloration at all, was found to be a mixture of predominantly Fe_3O_4 with some FeO on the unground surface (down to ~ 2 μm) but was pure FeO (within the limits of detection) after grinding. The above indicates that the oxygen reacts very rapidly with either the growing FeO or Fe_3O_4, forming Fe_2O_3 if the oxygen concentration is high enough. At the end of the reactor, there is either no oxygen left to oxidize the last sample or it is at too low a concentration to form a separate phase of Fe_2O_3.

This was reinforced by an experiment with about 10 times less oxygen (0.13%, run 125). In this run, only the inlet half of the first sample was reddish; the back half of sample 1 and all other samples was gray. In the X-ray studies, the brown surface showed major peaks of Fe_3O_4 and Fe_2O_3; after grinding, the major peaks in the sample were those of Fe_3O_4, with minor peaks of Fe_2O_3. All the other samples in this run showed only FeO if the conversion was below unity (samples 4 and 6) while that of high conversion (sample 5) showed Fe_3O_4 predominating the unground state, with FeO the main peak after grinding. Evidently, the oxygen in run 125 dropped below the critical level during the time it took the gas mixture to traverse the first sample. This level can not be measured in any simple way, as the system is so extremely reactive with gaseous oxygen.

Another effect of the oxygen is to increase dramatically the rate of FeO formation, even when the level of oxygen is below that needed to form detectable Fe_2O_3. This is shown by sample 6 in run 124, which was a 330-μm steel sample, of overall conversion of 0.424. Its X-ray spectrum showed mainly FeO after grinding, but its average growth rate was 70 μm/h as compared with the average value for the same steel of 27 μm/h, in runs 119, 121, and 122. The same effect is seen in run 125 for the iron foils as they grew at rates from 47 to 33 μm/h, compared to the usual rate of 22.4 μm/h. Furthermore, the rate decreased steadily from the inlet, the highest rate on sample 2 ($FeO_{0.943}$) being 47 μm/h and the lowest for sample 4 ($FeO_{0.66}$) being 33 μm/h. Samples 1 and 5, of 50.8 μm in thickness, were converted beyond FeO to mixtures of FeO, Fe_3O_4, and Fe_2O_3. Again, we find a rate increase (sample 125-4, 33 μm/h) without the detectable formation of Fe_2O_3 or Fe_3O_4. The sample nearest the exit in this run (sample 6, 330 μm, steel) also showed a small increase in rate of FeO growth (30 vs. 27 μm/h).

Scanning Electron Microscopy Data. In some of our early work, we discussed[16,21] the mechanism of filamentous carbon formation on FeO. It was suggested that the reason for the high activity of FeO compared to that of Fe and Fe_2O_3 was that FeO, having a defect structure, was easy to reduce to porous iron. We will discuss briefly the striking differences between filamentous carbon production on FeO, on the one hand, and on pure iron foils on the other. In our previous paper, the average rate of coke formation of iron was given as 11.4 mg of carbon per square centimeter (of starting surface) per hour (of exposure to ethane at 700 °C). For FeO, the average rate was 138 (mg/cm^2)/h, or about 12 times as fast. However, there is more to the phenomenon than just the average rate of filamentous coke formation. The earlier work in a controlled-atmosphere scanning electron microscope[16] used acetylene at 0.3 Torr as the coking agent. It was noted after 10 min the iron specimen stopped growing carbon, while FeO not only catalyzed the carbon formation at a rate faster than that of the metal but also continued to react with the acetylene for times of up to 2 h.

Our recent SEM photographs show the initiation of this process in more detail. Figure 14 shows the beginning state of the surface of an FeO sample (121-4), which was close to fully converted FeO, showing its complex crystalline morphology. Figure 15 shows the surface after 10 min of coking with ethane at atmospheric pressure at 700 °C. It will be seen that both images at 2100× clearly show the porosity created in the FeO surface as the reduction to Fe takes place. The backscattered images show good contrast between elements of varying atomic number; the elements of higher atomic number (e.g. iron) are lighter in the photographs than elements of low atomic number (e.g. carbon). Thus, the white dots in the lower photograph of Figure 16 (supplementary material) are the iron particles that have catalyzed the growth of the filaments.

Further details of the reduction process are shown in Figure 17 (supplementary material). It will be seen that as one moves to the right from the fracture in the middle of the photograph, the narrow light area is the original FeO (unreduced, composition measured by in situ EDAX analysis in the SEM), then there is a gray region, which is the porous iron produced by reducing the FeO. The black layer on the right of the sample is the filamentous coke. Analysis of the latter showed iron to be present as well as carbon. These above observations would seem to confirm our earlier[16] suspicions that the formation of porous iron is the cause of the high catalytic activity of FeO.

Conclusions

A new method for the low-temperature synthesis of pure FeO has been developed; it involves the use of pure steam atmospheres above 540 °C. To get reasonable growth rates, temperatures above 700 °C have to be used. For example, the growth rate on pure iron foils at 700 °C is 2.3 μm/h, while it is 20 μm/h at 800 °C. The purity of the water does not seem to be critical; we made an attempt to make potassium-doped FeO by the use of potassium solutions to generate the steam, but no potassium was found by Auger analysis in the FeO made this way.

It is well-known that the main oxide of iron formed in the presence of iron, water, and air is Fe_2O_3, so we investigated the effect of adding oxygen to the steam. At the low levels obtained by using nondeaerated water, no Fe_2O_3 was detected, and pure FeO was made at the normal growth rate. For additions of 1.44 and 0.13% O_2 (from added air), we found a mixture of FeO, Fe_3O_4, and Fe_2O_3 to form. The reaction of the oxygen with the iron was extremely rapid at 800 °C, as the degree to which the oxygen went down the reactor could readily be followed by the brown color of the Fe_2O_3. However, even when too low an O_2 concentration was present to form either Fe_2O_3 or Fe_3O_4, the presence of the oxygen could be detected by the higher growth rate of the FeO. At present, as the use of pure steam is so simple, we have not attempted to study the controlled addition of oxygen to speed up the FeO growth rate.

We have made the significant observation that FeO can only be made this way as long as free, zerovalent iron is present. This means that the starting geometry of the sample is critical. For example, foils, flat plates, or cylinders are suitable, while powders, unless monodisperse, are not. As soon as the free iron is consumed, so that the sample becomes entirely FeO, then we find by X-ray analysis that Fe_3O_4 begins to form on the outside surface of the FeO. If left long enough, the FeO will then completely transform into Fe_3O_4. Hence, it is obvious that if we begin with a normal iron powder, which had a wide range of particle sizes, we will end up with a mixture of FeO and Fe_3O_4 and, possibly, unreacted iron.

The above implies that the mechanism of FeO formation is that, after a surface layer of FeO is formed, the iron must diffuse outward through the FeO to react with the oxygen at the outside surface. When all the metal has been oxidized to FeO, the steam then reacts with the surface of the FeO, converting it to Fe_3O_4. In this instance, it seems most likely that the oxygen diffuses inward through the growing Fe_3O_4.

It was found that FeO has a unique surface property. When it is contacted with hydrocarbons at elevated temperatures for residence times such that only filamentous carbon is formed, the FeO is then more than 1 order of magnitude more active a catalyst than pure iron. This is despite the fact that the FeO has to be reduced to iron before it is active in carbon filament formation. We have now shown that the reason for this is that extremely porous iron is formed by the reduction of the FeO, as shown by scanning electron microscope studies. This porosity is due to the removal of oxygen from the FeO lattice.

(21) Baker, R. T. K.; Yates, D. J. C.; Dumesic, J. A. *Filamentous Carbon Formation Over Iron Surfaces*; Albright, L. A., Baker, R. T. K., Eds.; ACS Symposium Series 202; American Chemical Society: Washington, DC, 1982.

Acknowledgment. We wish to thank Michelle Modrick of Exxon Research and Engineering Co. for help and advice with the X-ray measurements, and in particular with calculating the penetration depth of the X-rays into the FeO samples.

Registry No. Fe, 7439-89-6; H_2O, 7732-18-5; O_2, 7782-44-7; FeO, 1345-25-1.

Supplementary Material Available: A summary of X-ray diffraction data (Table II) and figures showing the rate of formation of FeO as a function of water flow (Figure 2), X-ray spectra of sample 125-5 and reference spectra of Fe_3O_4 and FeO (Figure 9 and 10), SEM photographs of the coked FeO surface (Figure 16), and SEM photographs of a fractured section of FeO after coking (Figure 17) (7 pages). Ordering information is given on any current masthead page.

Contribution from the Guelph-Waterloo Centre for Graduate Work in Chemistry, Waterloo Campus, Department of Chemistry, University of Waterloo, Waterloo, Ontario N2L 3G1, Canada, Istituto di Chimica Generale ed Inorganica, Università di Torino, 10125 Torino, Italy, and Istituto di Chimica Generale ed Inorganica, Università di Parma, and Centro di Studio per la Strutturistica Diffrattometrica del CNR, 43100 Parma, Italy

Conversion of a μ-η^2-Acetylide to a μ-η^2-$\parallel$-Acetylene via Successive Nucleophilic Additions. X-ray Structure of $Os_2(CO)_6[\mu$-η^2-C{C(NH-*t*-Bu)(S-*n*-Bu)}CPh$](\mu$-$PPh_2)$

Andrew A. Cherkas,[1a] Arthur J. Carty,*[1a] Enrico Sappa,[1b] Maria Angela Pellinghelli,[1c] and Antonio Tiripicchio[1c]

Received March 24, 1987

The diosmium acetylide complex $Os_2(CO)_6(\mu$-η^2-C≡CPh$)(\mu$-$PPh_2)$ (**1**) has been converted in two stages to the parallel acetylene derivative $Os_2(CO)_6[\mu$-η^2-C{C(NH-*t*-Bu)(S-*n*-Bu)}CPh$](\mu$-$PPh_2)$ (**3**). Nucleophilic attack at carbon by *t*-BuNC afforded Os_2-$(CO)_6[\mu$-η^2-C{CN-*t*-Bu}CPh$](\mu$-$PPh_2)$ (**2**), and subsequent elaboration of **2** with *n*-BuSH gave, via S–H addition to the isocyanide C≡N bond, the compound **3**. Complex **3** crystallizes in the orthorhombic space group $P2_12_12_1$ with a = 18.276 (9) Å, b = 19.307 (8) Å, c = 10.265 (5) Å, V = 3622 (3) Å^3, Z = 4, $F(000)$ = 1928, and μ = 71.60 cm^{-1}. The structure was solved and refined to R and R_w values of 0.044 and 0.049 by using 2451 ($I \geq 2\sigma(I)$) unique observed data measured on a Siemens AED diffractometer. The molecular structure of the binuclear molecule (Os–Os = 2.813 (3) Å) contains a phosphido bridge (Os(1)–P–Os(2) = 74.1 (2)°) and a dipolar, disubstituted μ-η^2-$\parallel$-acetylene with substituents Ph and C(NH-*t*-Bu)(S-*n*-Bu). The acetylide triple bond length in **1** (1.228 (18) Å) increased to 1.28 (2) Å in **3**.

Introduction

The interrelationships and reactivity patterns of multisite-bound unsaturated ligands are currently the focus of considerable attention in organometallic chemistry.[2] The acetylide ligand –C≡C—R occupies a significant position in the hierarchy of small unsaturated molecules for a number of reasons: (i) the acetylide anion is isoelectronic with CO, and its coordination behavior in polynuclear systems frequently resembles that of multisite-bound CO;[3] (ii) as a two-carbon fragment, the acetylide is a potential source of other important hydrocarbyls including vinylidene, vinyl, alkylidene, and alkylidyne groups; (iii) the acetylide ligand is unrivaled in its versatility as a bridging hydrocarbyl, with symmetrical μ, μ-η^2, μ_3-η^2, and μ_4-η^2 bonding modes all well established.[4] We have recently documented a number of C–C,[5] C–N,[6], and C–P[7] bond-forming reactions on μ_n-η^2-acetylides, and in this paper we wish to report the conversion of $Os_2(CO)_6(\mu$-η^2-C≡CPh$)(\mu$-$PPh_2)$ (**1**) to the acetylene complex $Os_2(CO)_6[\mu$-η^2-C{C-(NH-*t*-Bu)(S-*n*-Bu)}CPh$](\mu$-$PPh_2)$ (**3**) via the strategy of successive nucleophilic additions of *t*-BuNC and *n*-BuSH. We note that Shriver[8] has recently demonstrated the transformation of a ketenylidene via a μ_3-η^2-acetylide to a μ_3-η^2-$\perp$-acetylene on an Fe_3 cluster.

Experimental Section

All manipulations were carried out on a double manifold by using standard Schlenk techniques. Solvents were dried as follows and distilled under nitrogen prior to usage: hexane and heptane, over $LiAlH_4$; benzene and cyclohexane, over $Na^+Ph_2CO^-$. Column chromatography utilized 100–200-mesh Florisil. IR spectra were measured on a Perkin-Elmer 180 instrument using matched sodium chloride solution cells of 0.5-mm path length. NMR spectra were recorded on Bruker AM-250 (^{1}H, 250 MHz; ^{31}P, 101.3 MHz) or WH-400 (^{1}H, 400 MHz; ^{31}P, 162.0 MHz; ^{13}C, 100.6 MHz) instruments. Chemical shifts are referenced to TMS and 85% H_3PO_4.

Syntheses: $Os_2(CO)_6[\mu$-η^2-C{CN-*t*-Bu}CPh$](\mu$-$PPh_2)$ (2). The binuclear acetylide **1**[9] (30 mg, 0.036 mmol) was dissolved in *n*-heptane (7 mL) and a solution of *tert*-butyl isocyanide (38.8 mg, 0.47 mmol) in heptane (5 mL) added. The pale yellow solution gradually darkened, and a yellow precipitate formed. When IR monitoring indicated complete consumption of **1**, a few drops of benzene were added to dissolve the precipitate, the solution was adsorbed onto Florisil, and the stained Florisil was added to the top of a 7 × 1.5 cm column of the same material. The only

(1) (a) Guelph-Waterloo Centre. (b) Università di Torino. (c) Università di Parma.
(2) For a selection of recent references see: (a) Casey, C. P.; Roddick, D. M. *Organometallics*, **1986**, *5*, 436. (b) Gracey, B. P.; Knox, S. A. R.; MacPherson, K. A.; Orpen, A. G.; Stobart, S. R. *J. Chem. Soc., Dalton Trans.* **1985**, 1935. (c) Vites, J. C.; Jacobsen, G.; Dutta, T. K.; Fehlner, T. P. *J. Am. Chem. Soc.* **1985**, *107*, 5563. (d) Beanan, L. R.; Keister, J. B. *Organometallics* **1985**, *4*, 1713. (e) Sailor, M. J.; Shriver, D. F. *Organometallics* **1985**, *4*, 1476. (f) Nuel, D.; Dahan, F.; Mathieu, R. *J. Am. Chem. Soc.* **1985**, *107*, 1658. (g) Morrison, E. D.; Steinmetz, G. R.; Geoffroy, G. L.; Fultz, W. C.; Rheingold, A. L. *J. Am. Chem. Soc.* **1984**, *106*, 4783. (h) Holmgren, J. S.; Shapley, J. R. *Organometallics* **1985**, *4*, 793. (i) McGhee, W. D.; Bergman, R. G. *J. Am. Chem. Soc.* **1986**, *108*, 5621.
(3) (a) Carty, A. J. *Pure Appl. Chem.* **1982**, *54*, 113 and references therein. (b) Nast, R. *Coord. Chem. Rev.* **1982**, *47*, 89.
(4) See for example: (a) μ: Carty, A. J.; Taylor, N. J.; Smith, W. F. *J. Chem. Soc., Chem. Commun.* **1979**, 750. (b) μ-η^2: Smith, W. F.; Yule, J.; Taylor, N. J.; Paik, H. N.; Carty, A. J. *Inorg. Chem.* **1977**, *16*, 1593. Nubel, P. O.; Brown, T. L. *Organometallics* **1984**, *3*, 29. (c) μ_3-η^2: Carty, A. J.; MacLaughlin, S. A.; Taylor, N. J. *J. Organomet. Chem.* **1981**, *204*, C27. Sappa, E.; Gambino, O.; Milone, L.; Cetini, G. *J. Organomet. Chem.* **1972**, *39*, 169. (d) μ_4-η^2: MacLaughlin, S. A.; Taylor, N. J.; Carty, A. J. *Organometallics* **1983**, *2*, 1194. (e) Weatherell, C.; Taylor, N. J.; Carty, A. J.; Sappa, E.; Tiripicchio, A. *J. Organomet. Chem.* **1985**, *291*, C9.
(5) (a) Carty, A. J.; Mott, G. N.; Taylor, N. J. *J. Organomet. Chem.* **1981**, *212*, C54. (b) MacLaughlin, S. A.; Johnson, J. P.; Taylor, N. J.; Carty, A. J.; Sappa, E. *Organometallics* **1983**, *2*, 352. (c) Nucciarone, D.; Taylor, N. J., Carty, A. J. *Organometallics* **1986**, *5*, 1179. (d) Gervasio, G.; Sappa, E.; Manotti Lanfredi, A. M.; Tiripicchio, A. *Inorg. Chim. Acta* **1983**, *68*, 171.
(6) Mott, G. N.; Carty, A. J. *Inorg. Chem.* **1983**, *22*, 2726.
(7) Carty, A. J.; Ferguson, G.; Khan, M. A.; Mott, G. N.; Roberts, P. J.; Taylor, N. J. *J. Organomet. Chem.* **1978**, *149*, 345.
(8) Hriljac, J. A.; Shriver, D. F. *Organometallics* **1985**, *4*, 2225.
(9) Cherkas, A. A.; MacLaughlin, S. A.; Taylor, N. J.; Carty, A. J., unpublished results.

0020-1669/87/1326-3201$01.50/0